Nonlinear Dyn
DOI 10.1007/s11071-014-1627-3

ORIGINAL PAPER

Energy efficiency in friction-based locomotion mechanisms for soft and hard robots: slower can be faster

Xuance Zhou · Carmel Majidi · Oliver M. O'Reilly

Received: 18 March 2014 / Accepted: 29 July 2014

Abstract Many recent designs of soft robots and nano-robots feature locomotion mechanisms that cleverly exploit slipping and sticking phenomena. These mechanisms have many features in common with peristaltic locomotion found in the animal world. The purpose of the present paper is to examine the energy efficiency of a locomotion mechanism that exploits friction. With the help of a model that captures most of the salient features of locomotion, we show how locomotion featuring stick-slip friction is more efficient than a counterpart that only features slipping. Our analysis also provides a framework to establish how optimal locomotion mechanisms can be selected.

Keywords Hybrid dynamical systems · Piecewise-smooth dynamical systems · Stick-slip friction · Anchoring · Peristaltic locomotion · Worm-like motion · Robotics

X. Zhou · O. M. O'Reilly (✉)
Department of Mechanical Engineering, University of California at Berkeley, Berkeley, CA 94720-1740, USA
e-mail: oreilly@berkeley.edu

X. Zhou
e-mail: xuance.zhou@berkeley.edu

C. Majidi
Department of Mechanical Engineering, Carnegie Mellon University, Pittsburg, PA 15213, USA
e-mail: cmajidi@andrew.cmu.edu

1 Introduction

Recent advancements in the field of robotics include the development of soft robots [10] and micro-robots [4,5,20,23]. For some soft robot designs, such as the recent pneumatic quadruped in Shepherd et al. [19], locomotion can be achieved by coordinated sticking and slipping of the limbs. A similar mechanism can be found in certain micro-robots, such as the ETH-Zürich Magmite [8,14,15], UT-Arlington ARRIpede [12,13], Dartmouth scratch-drive MEMS robot [3], and magentic micro-robot from Carnegie-Mellon University [17]. At the macroscale, stick-slip locomotion is also featured in the Capsubot from Tokyo's Denki University [9] and the Friction Board System [21]. It is also of interest to note that locomotion mechanisms featuring sticking and slipping of limbs can also be related to the limbless crawling (peristaltic locomotion [7,11]) observed in a wide variety of species and bio-inspired robots [16,18] where anchoring (sticking) is realized either by bristles or mucus [2].

The wealth of designs and implementations in the aforementioned works make it difficult to gain a perspective on the overall energy efficiency of a locomotion scheme controlled by friction. A commercially available toy, shown in Fig. 1, enables us to see the features of robot locomotion that suffice to examine this efficiency. The toy horse has three main components: two limbs joined by a pair of hinge joints and an air bellows. As documented in Fig. 1c, by pumping on the bellows, the toy locomotes forward. One model

Published online: 19 August 2014

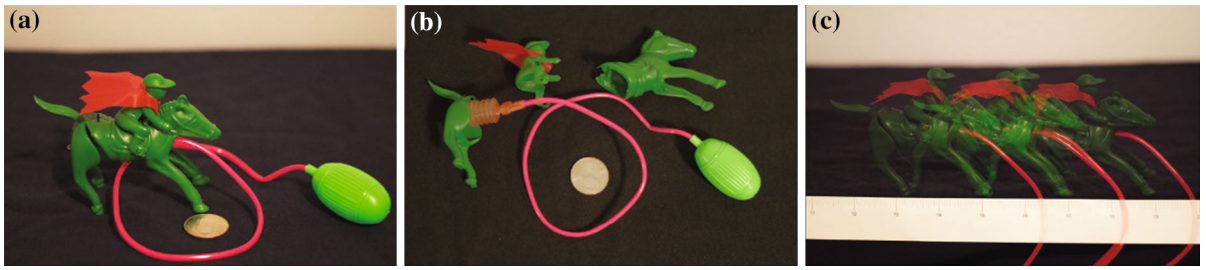

Fig. 1 Locomotion of a toy horse. **a** Photo of the stationary toy. **b** Photo of the primary components of the toy horse. **c** A series of time-lapsed images of the toy horse in motion. The coin in (**a**) and (**b**) is a US quarter

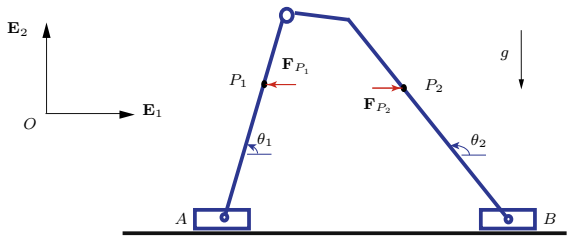

Fig. 2 Schematic of a two-degree-of-freedom model for the toy horse shown in Fig. 1. The figure also indicates the forces $\mathbf{F}_{P_1}$ and $\mathbf{F}_{P_2}$ exerted on the respective links by the pneumatic actuator

for this toy is to represent it as the two-link mechanism shown in Fig. 2. The forces due to the bellows (actuator) are modeled by the forces $\mathbf{F}_{P_1}$ and $\mathbf{F}_{P_2}$ acting on the links. As these forces are varied, the normal forces on the end masses m_A and m_B change. The resulting change in the normal forces can induce changes to the friction forces acting on the end masses. If the system is properly designed and the forces $\mathbf{F}_{P_1}$ and $\mathbf{F}_{P_2}$ are properly coordinated, then, as illustrated in Fig. 3, a net forward motion of the center of mass of the system can be achieved.

We consider the locomotion shown in Fig. 3 to be an example of stick-slip locomotion (SSL). However, as we subsequently discovered, it is also possible to achieve locomotion with both limbs in a perpetual state of sliding. We define this locomotion as sliding locomotion (SL). It is of interest to us to examine how both of these types of locomotion schemes can be actuated, which one of them is more energy efficient, and which one of them enables faster locomotion. To perform such an analysis, we found it essential to simplify the model shown in Fig. 2 to the two mass system shown in Fig. 4. In this representation, the actuator is modeled as a spring with a variable initial length $\ell_0(t)$. The spring is also inclined so that changing the initial length induces changes to the normal forces on the masses. By changing the angle of inclination for a given $\ell_0(t)$, the center of mass of the system can be made to move backwards or forwards.

While the majority of works in the application area of interest have addressed hardware design and fabrication, there is an ever increasing number of papers devoted to a systematic analysis of relevant theoretical models (see, e.g., [1,6,9,22,24]). Such analysis is challenging because the dynamics are governed by non-smooth hybrid dynamical systems and recourse to numerical methods is necessary. The present paper expands such efforts by examining the energetics and performance of devices that feature friction-induced locomotion.

The paper is organized as follows: In the next section, Sect. 2, a two-degree-of-freedom model for the locomotion system is described. The model is excited internally by changing the unstretched spring length $\mathcal{L}_0(t)$. The interaction of the resulting normal and friction forces then leads to locomotion. In Sect. 3, this locomotion is classified into two types and the influence of some system parameters on the locomotion is discussed. We then turn to examining the energy efficiency of the SSL and SL mechanisms. Our numerical analysis features a range of simulations with varying system parameters. As in refs. [1,24], we show how uneven friction force distribution can lead to locomotion of the center of mass. Our analyses conclude with a discussion of the effects of mass distribution in Sect. 5. The paper concludes with a set of design recommendations for balancing time taken by the model to travel a given distance subject to a given energy dissipation.

2 A simple model

While the exploitation of friction to generate locomotion is well known (see, e.g., [4]), analyzing simple

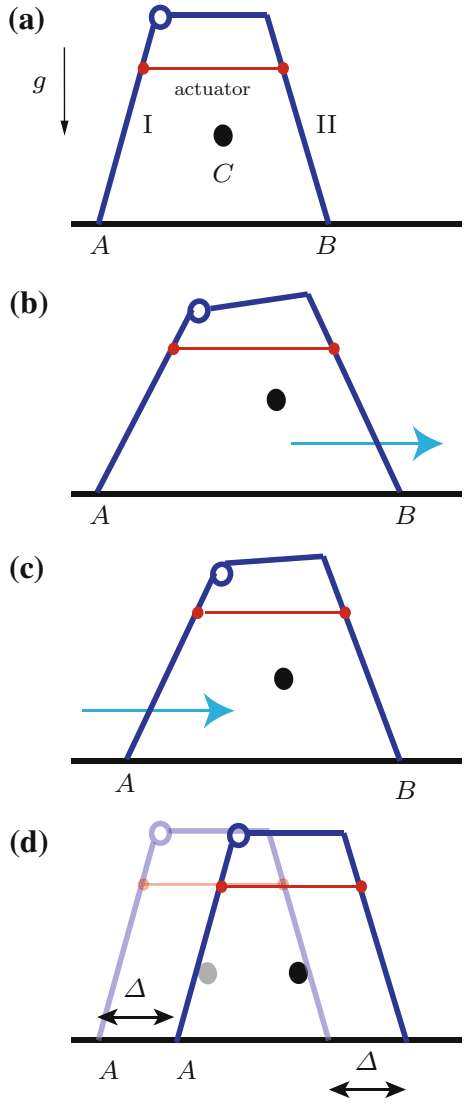

Fig. 3 Illustration of the locomotion for the model system shown in Fig. 2. In **a** the system is at rest, then in **b** the actuator extends and the link labeled *II* moves forward while link *I* stays fixed. In **c**, the point *A* stays fixed, the actuator retracts and link *I* slips. The net motion Δ of the system after one cycle is shown in (**d**). In these figures the point *C* is the center of mass of the system

models to examine the features of the implementation of this locomotion mechanism are rare. The simplest model we found that could explain the salient features and some of the challenges of SL and SSL were a two-degree-of-freedom mass-spring system shown in Fig. 4a. As can be seen from the figure, the masses are connected by a spring and are both free to move on a horizontal surface.

The spring element in the model features an unstretched length $\mathcal{L}_0$ that is to be controlled. This feature of the model mimics the bellows in the toy horse and is similar to the active spring used in the recent work [22] to explain some features of peristaltic locomotion. We assume that the spring element is linear and exerts a force $-\mathbf{F}_s$ on m_1 and $\mathbf{F}_s$ on m_2:

$$\mathbf{F}_s = -K\left(\mathcal{L} - \mathcal{L}_0(t)\right)\left\{\left(\frac{X_2 - X_1}{\mathcal{L}}\right)\mathbf{E}_1 + \frac{D}{\mathcal{L}}\mathbf{E}_2\right\}, \tag{1}$$

where X_1 is the displacement of the mass M_1 and X_2 is the displacement of the mass M_2. The extended length $\mathcal{L}$ of the spring features a vertical offset D:

$$\mathcal{L} = \sqrt{(X_2 - X_1)^2 + D^2}. \tag{2}$$

The corresponding angle between the directions of $\mathbf{F}_s$ and a unit vector in the horizontal direction, $\mathbf{E}_1$, is

$$\theta = \arcsin\frac{D}{\mathcal{L}}, \quad 0 \le \theta < \frac{\pi}{2}. \tag{3}$$

We choose the origin so that the position of the centers of mass for M_1 and M_2 are 0 in the vertical $\mathbf{E}_2$ direction. Finally, the position vector of the center of mass C is

$$X\mathbf{E}_1 = \frac{M_1X_1 + M_2X_2}{M_1 + M_2}\mathbf{E}_1. \tag{4}$$

The motion C is crucial to characterizing the efficiency of the locomotion scheme.

To mimic the effect of varying normal force that would be present in a more realistic model of the actual system, we have tilted the spring at an angle θ to the horizontal. In this way, varying $\mathcal{L}_0$ induces a change in the normal forces $N_{1,2}$ on the individual masses:

$$N_1 = M_1g + \mathbf{F}_s \cdot \mathbf{E}_2, \quad N_2 = M_2g - \mathbf{F}_s \cdot \mathbf{E}_2. \tag{5}$$

If there is sufficient variation, then it can enable a transition to and from static and dynamic friction. If $\mu_s > \mu_d$, then this transition can produces a motion of the mass particles. For instance, in SSL, a recurring pattern of transitions where M_1 is stuck and M_2 moves, followed by M_2 being stuck and M_1 moving toward M_2 can occur. We also observe from Fig. 4b that if ℓ_0 is

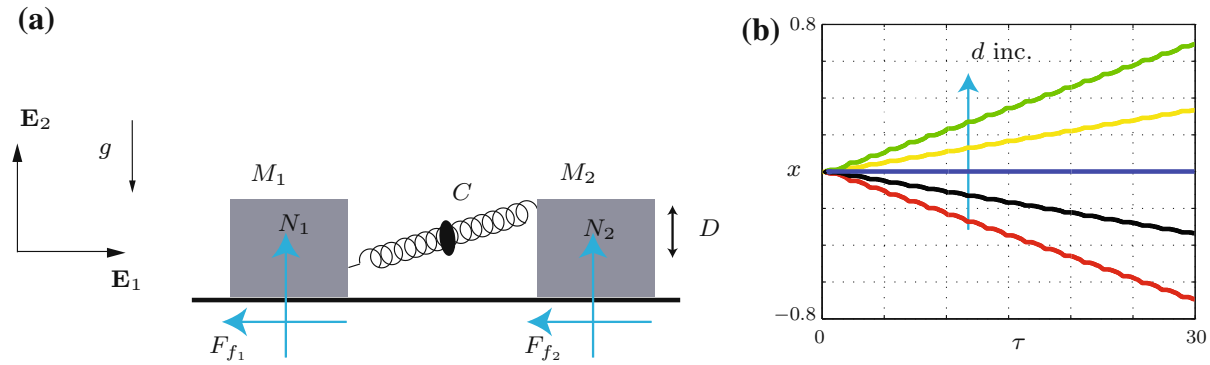

Fig. 4 A simple two-degree-of-freedom model used to analyze SL and SSL. **a** Schematic of the model showing the normal and friction forces. **b** The displacement x of the center of mass C of the system for various values of d and $\ell_0(t) = 0.05\sin(\pi t) + 3$. Referring to (1), the parameters for this model are $K = 50$, $m_1 = m_2 = 1$, $\mu_s = 0.7$, $\mu_k = 0.5$, and $d = D/\hat{\mathcal{L}}$ is assigned the values of -0.5, -0.25, 0.0, 0.25, and 0.50

properly controlled, then locomotion of the center of mass C of the system is possible.

It is convenient to define the normalized vertical offset $d = D/\hat{\mathcal{L}}$, where $\hat{\mathcal{L}}$ is a suitable length scale. Possible choices of $\hat{\mathcal{L}}$ include D and $\mathcal{L}_0(t = 0) \neq 0$. As can be seen from the results shown in Fig. 4b, when $d > 0\,(< 0)$, then the center of mass of the model moves forward (backward) and is stationary when $d = 0$. In compiling the results shown in this figure, we choose $\mathcal{L}_0(t) = A\sin(\pi t) + \bar{\mathcal{L}}$. It is natural to ask what is the optimal $\mathcal{L}_0(t)$ needed to achieve locomotion for a given average speed of the center of mass C? A related question is what is the optimal $\mathcal{L}_0(t)$ to have the system perform a prescribed task with minimal power expenditure?

2.1 Equations of motion

Before we derive the equations of motion, we define a dimensionless time $\tau = t\sqrt{g}/\hat{\mathcal{L}}$ and introduce some new dimensionless parameters

$$
\begin{aligned}
&m_1 = \frac{M_1}{M}, \quad m_2 = \frac{M_2}{M},\\
&x_1 = \frac{X_1}{\hat{\mathcal{L}}}, \quad x_2 = \frac{X_2}{\hat{\mathcal{L}}}, \quad \ell = \frac{\mathcal{L}}{\hat{\mathcal{L}}},\\
&a = \frac{A}{\hat{\mathcal{L}}}, \quad \ell_0 = \frac{\mathcal{L}_0}{\hat{\mathcal{L}}}, \quad \bar{\ell} = \frac{\bar{\mathcal{L}}_0}{\hat{\mathcal{L}}},\\
&\omega = \Omega\frac{\hat{\mathcal{L}}}{g}, \quad k = \frac{K\hat{\mathcal{L}}}{Mg}, \quad c = \frac{C}{M}\sqrt{\frac{\hat{\mathcal{L}}}{g}},\\
&n_1 = \frac{|N_1|}{Mg}, \quad n_2 = \frac{|N_2|}{Mg},
\end{aligned}
\tag{6}
$$

where we choose $M = (M_1 + M_2)/2$. In the following equations, the $\dot{()}$ indicates a differentiation with respect to τ.

The equations of motion for the simple model form a hybrid system with state-dependent switching. Here, we treat the friction as Coulomb friction. For a given mass M_i, the pair of conditions required for static friction are

Condition 1. $\dot{x}_i(t) = 0$.
Condition 2. $|k\,(\ell - \ell_0)\cos(\theta)| \leq \mu_s n_i(t)$.

Here, μ_s is the coefficient of static friction. Based on the pair of conditions, the switching sets can be defined as follows:

$$
\begin{aligned}
\mathcal{B}_1 &= \{(x_1, \dot{x}_1, x_2, \dot{x}_2) | \dot{x}_1 = 0 \quad \text{and} \quad |f_x| \leq \mu_s n_1\},\\
\mathcal{B}_2 &= \{(x_1, \dot{x}_1, x_2, \dot{x}_2) | \dot{x}_2 = 0 \quad \text{and} \quad |f_x| \leq \mu_s n_2\}.
\end{aligned}
\tag{7}
$$

Here,

$$
f_x = k\,(\ell - \ell_0)\cos(\theta), \quad \text{and}
$$
$$
\theta = \arcsin\left(\frac{d}{\sqrt{(x_2 - x_1)^2 + d^2}}\right). \tag{8}
$$

Using the switching sets, the equations of motion of the system can be expressed as follows:

$$
\begin{aligned}
&m_1\ddot{x}_1 = 0, \quad (x_1, \dot{x}_1, x_2, \dot{x}_2) \in \mathcal{B}_1,\\
&m_2\ddot{x}_2 = 0, \quad (x_1, \dot{x}_1, x_2, \dot{x}_2) \in \mathcal{B}_2,\\
&\left.\begin{aligned}
m_1\ddot{x}_1 + c\dot{x}_1 - f_x + \tfrac{\dot{x}_1}{|\dot{x}_1|}\mu_d n_1 = 0\\
m_2\ddot{x}_2 + c\dot{x}_2 + f_x + \tfrac{\dot{x}_2}{|\dot{x}_2|}\mu_d n_2 = 0
\end{aligned}\right\} \quad (x_1, \dot{x}_1, x_2, \dot{x}_2) \notin \mathcal{B}_{1,2}.
\end{aligned}
\tag{9}
$$

The dimensionless total energy e of the system is

$$e = \frac{1}{2}m_1\dot{x}_1^2 + \frac{1}{2}m_2\dot{x}_2^2 + \frac{1}{2}k\left(\sqrt{(x_2 - x_1)^2 + d^2} - \ell_0\right)^2. \tag{10}$$

2.2 Analytical modes and natural frequencies

We expect four modes of behavior for the two-degree-of-freedom system:

Mode 0. m_1—stick, m_2—stick;
Mode 1. m_1—slip, m_2—slip;
Mode 2. m_1—slip, m_2—stick;
Mode 3. m_1—stick, m_2—slip.

It is convenient to define four natural frequencies that pertain to the case where $d = 0$ (i.e., the spring is horizontal) and the system dynamics are assumed to be linear. In this case, for Mode 1, we expect the system response to contain the natural frequency ω_{n_1} along with the rigid body mode ω_0:

$$\omega_0 = 0, \quad \omega_{n_1} = \sqrt{\frac{k\,(m_1 + m_2)}{m_1 m_2}}. \tag{11}$$

For Modes 2 and 3, the system shoud behave as a single mass system whose natural frequencies are, respectively,

$$\omega_{n_2} = \sqrt{\frac{k}{m_1}}, \qquad \omega_{n_3} = \sqrt{\frac{k}{m_2}}. \tag{12}$$

For the majority of the subsequent analyses, we set $m_1 = m_2$. Thus, $\omega_{n_2} = \omega_{n_3}$.

2.3 Internal excitation

In many of the applications of interest, the motion is controlled by varying a physical parameter of the system. For example in the toy horse shown in Fig. 1, the bellows serves as a spring of time-varying length, in the soft robot in Shepherd et al. [19], pneumatic cylinders are used to change an intrinsic curvature, and in peristaltic locomotion a traveling wave is used to induce changes to the structure's contact geometry [22]. To model these effects as simply as possible, we assume that the two-degree-of-freedom system is excited by a time dependent varying intrinsic length

$$\ell_0 = a\sin(\omega t) + \bar{\ell}. \tag{13}$$

In applications, this type of excitation could be realized either by a pneumatic cylinder, elastic deformation, or electromagnetic fields. Admittedly, other choices of the function $\ell_0(t)$ are possible and so our numerical investigation is not exhaustive. Indeed, within the context of the current system, it would be useful to develop a framework by which the optimal $\ell_0(t)$ that would minimize energy consumption while still ensuring that certain performance metrics are satisfied.

3 Two types of locomotion: SL and SSL

In simulations of the simple model presented in Sect. 2, two types of motion are anticipated: either stick-slip locomotion (SSL) or slip locomotion (SL). These two representative locomotion behaviors, which are discussed extensively in the sequel, are shown in Fig. 5.

What distinguishes SL from SSL is that for the latter one or more of the masses stick for discrete intervals of time during the motion. That is, for SSL, $\exists i \in \{1, 2\} : \dot{x}_i(t) = 0$ and $|k\,(\ell - \ell_0)\cos(\theta)| \leq \mu_s n_i(t)\,\forall t \in [T_1, T_2]$. In order for this pair of conditions to be satisfied, we found that we need the excitation frequency ω to be lower than the lowest

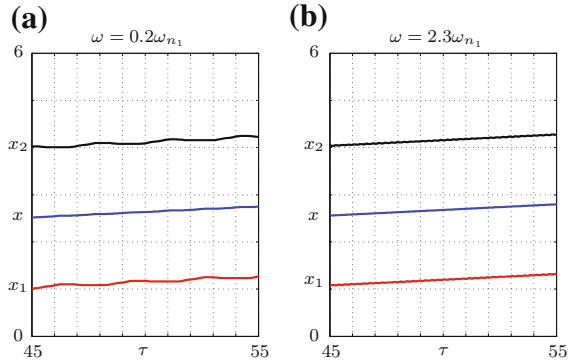

Fig. 5 Illustration of (**a**) SSL and (**b**) SL in the two-degree-of-freedom model governed by Eq. (9). In **a** the excitation frequency is $\omega = 0.2\omega_{n_1}$ and in **b** the excitation frequency is $\omega = 2.3\omega_{n_1}$. For both examples, the remaining parameters are $a = 0.05$, $k = 50$, $\bar{\ell} = 3$, $d = 0.5$, $c = 0.01$, $m_1 = m_2 = 1$, $\mu_k = 0.5$, $\mu_s = 0.7$ and $\omega_{n_1} = 10$

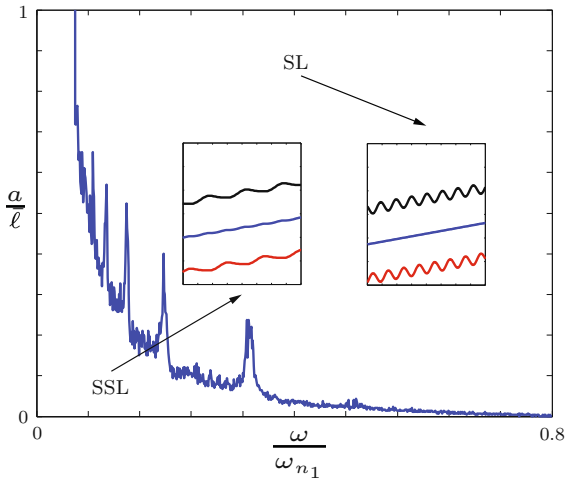

Fig. 6 A graph illustrating the region of SSL with the dimensionless amplitude a and dimensionless frequency ω as the varying parameters. The other parameter that are kept fixed are $k = 50, c = 0.01, \bar{\ell} = 3, d = 0.5, \mu_s = 0.7, \mu_k = 0.5, m_1 = m_2 = 1$, and $\omega_{n_1} = 10$

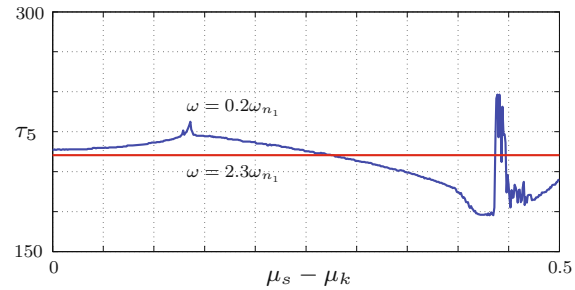

Fig. 7 Influence of $\mu_s - \mu_k$ on the dimensionless time τ_5 taken for the center of mass C to travel a distance of 5 dimensionless units with $\omega = 0.2\omega_{n_1}, a = 0.05, k = 50, c = 0.01, \bar{\ell} = 3, d = 0.5, m_1 = m_2, \mu_k = 0.5, \omega_{n_1} = 10$ and μ_s varying from 0.5 to 1.0

$\omega_{n_{1,2,3}}$ and the amplitude of excitation a should also be small. These results from our numerical simulations are shown in Fig. 6. In these numerical simulations, we categorize the motion as SL when no sticking behavior happens during a time interval $\Delta\tau = 25$ in the steady-state motion, otherwise, as SSL. Of all the parameters governing whether the locomotion was SSL or SL, ω was the most prepotent. As can be seen from Fig. 6, if ω is sufficiently large then the system's locomotion is SL. The discrete peaks in the transition curve seen in this figure also proved to be very sensitive to tolerances in our numerical integration schemes.

For all the above and subsequent numerical simulations, we set the initial conditions as

$$x_1(t=0) = 0, \quad x_2(t=0) = \bar{\ell},$$
$$\dot{x}_1(t=0) = \dot{x}_2(t=0) = 0. \tag{14}$$

The properties we characterize are based on the behavior of the system after the initial transients have subsided. We assume that a time period of at least 80 periods of the lowest natural frequency is sufficient of these transients to have decayed.

The second parameter which should play a key role in the occurrence of SSL is the static friction coefficient μ_s. To explore the effects of this parameter, we examined the relationship between the time taken τ_5 for the center of mass C to travel a distance of five dimensionless units and the difference between the static friction coefficient and the dynamic coefficient: $\mu_s - \mu_k$. In other words, we are interested in the effects of static friction on the average speed of locomotion. Referring to Fig. 7, we found that a larger static friction will help accelerate the system in a certain range. However, in general, the effects of varying the static friction coefficient $\mu_s \geq \mu_k$ are not significant when the dynamic coefficient μ_k is fixed.

4 Energetic considerations

An optimal locomotion scheme could be considered as one where a fixed distance is travelled in the shortest time while minimizing energy consumption. To examine optimality, we first need to define the energy consumption. For the system at hand, the energy consumption can be inspected in two equivalent manners. First, the energy consumed in actuating the spring is used to counterbalance the energy dissipated by friction and the linear damper. The energy dissipated e_d has the dimensionless representation:

$$e_d = \int_{\tau_1}^{\tau_2} \left\{ \mu_k n_1 |\dot{x}_1| + \mu_k n_2 |\dot{x}_2| + c\dot{x}_1^2 + c\dot{x}_2^2 \right\} \mathrm{d}\tau. \tag{15}$$

The second measure is to consider the work w done by the spring force. The work is balanced with the change in the total energy e of the system and the energy e_d dissipated by the system:

$$w = e_d + e(\tau = \tau_2) - e(\tau = \tau_1). \tag{16}$$

In the following numerical analysis, e_d will be used as a measure of the energy consumption. The advantage

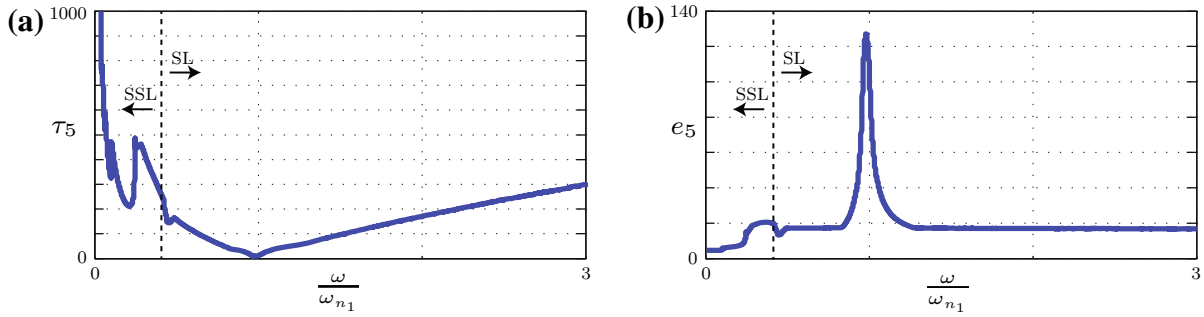

Fig. 8 Numerical results to analyze the efficiency of the model in Fig. 4 as a function of the excitation frequency ω. **a** Non-dimensionalized time τ_5 taken to travel a distance of five dimensionless units. **b** The corresponding non-dimensionalized energy consumption e_5 during the motion. The parameters for the model used to produce these results were $a = 0.05, \bar{\ell} = 3, d = 0.5, k = 50, c = 0.01, m_1 = m_2, \mu_k = 0.5, \mu_s = 0.7$ and $\omega_{n_1} = 10$

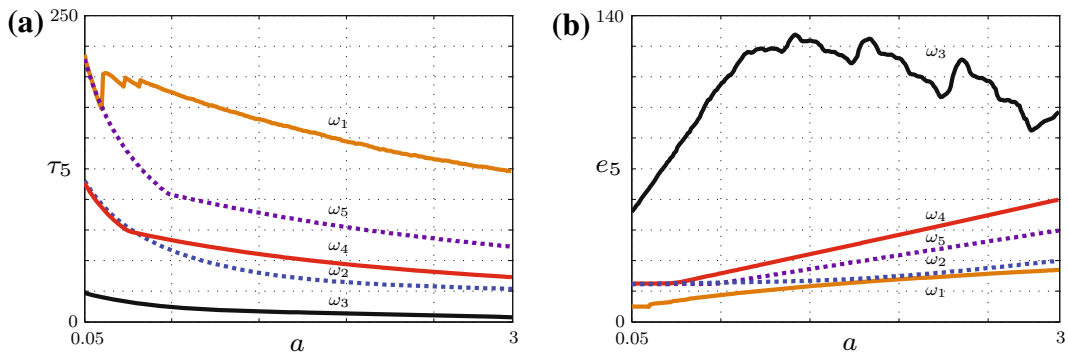

Fig. 9 Numerical results to analyze the efficiency of the model in Fig. 4 for a varying exciting frequency with three representative frequencies. **a** Non-dimensionalized time τ_5 travel a distance of 5 dimensionless units. **b** The corresponding dimensionless energy consumption e_5. The parameters for this model are $\bar{\ell} = 3, d = 0.5, k = 50, c = 0.01, m_1 = m_2 = 1, \mu_k = 0.5, \mu_s = 0.7$ and $\omega_1 = 2, \omega_2 = 6, \omega_3 = 9.5, \omega_4 = 16$ and $\omega_5 = 23$, respectively

of choosing e_d over w is that e_d not only indicates the amount of energy consumed in order to make the system move, but also shows the amount of energy converted to heat. Heat dissipation is often a non-trivial issue for MEMS devices which can be susceptible to thermal failure.

To explore efficiency, we considered the time τ_z taken for the center of mass C to travel a distance z and the corresponding energy e_z. We computed these metrics for a range of excitation frequencies ω and have compiled a representative selection of the results in Fig. 8. The results shown in Fig. 8 challenge our perception that it is always economical to excite a system at resonance. Clearly, one attains the minimum time to travel a given distance when ω is close to the frequency ω_{n_1} and there are also local minima near $\omega_{n_2} = \omega_{n_3}$. However, the maximum energy dissipated also occurs when ω is close to ω_{n_1}.

In the region $\omega/\omega_{n_1} < 0.3$ where SSL is the observed locomotion mechanism, several local minima in travel time τ_5 occur with minimal changes in e_5. However, there are several disadvantages for those minima in SSL region. First, these critical points are very sensitive to changes in ω and, second, the average speed doesn't compare to that when ω is close to ω_{n_1}. In general, the results in Fig. 8 indicate that energy efficiency can never be achieved without lowering the average speed of the center of mass C.

Another key factor in excitation is the amplitude a of the spring's intrinsic length $\ell_0(t)$. In order to draw some conclusions on the influence of a, five excitation frequencies were selected featuring two low frequencies (one with SSL and one featuring SL), one frequency near resonance and two high frequencies. On the whole, the trend in Fig. 9 agrees with the results shown in Fig. 8 that a higher average speed can only be achieved with a

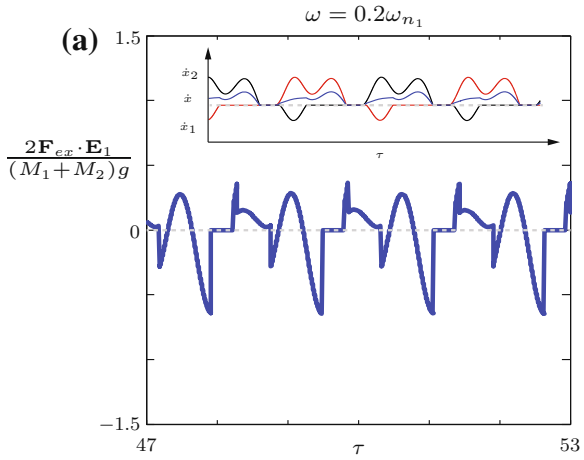

Fig. 10 Illustration of the force and velocity profiles for the two typical types of motion exhibited by the solutions to Eq. (9). In **a** the excitation frequency is $\omega = 0.2\omega_{n_1}$ and in **b** the excitation frequency is $\omega = 2.3\omega_{n_1}$. For both examples, the remaining parameters are $a = 0.05$, $k = 50$, $\bar{\ell} = 3$, $d = 0.5$, $c = 0.01$, $m_1 = m_2 = 1$, $\mu_k = 0.5$, $\mu_s = 0.7$, and $\omega_{n_1} = 10$

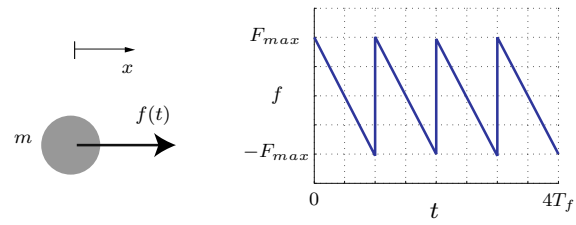

Fig. 11 Schematic of a particle m moving under the influence of a resultant periodic force $f(t)$. The sawtooth profile of f is also shown

higher concomitant energy dissipation.[1] One feature of particular interest in Fig. 9 is that when $a \leq 0.08$, the system substantially traveled the fixed distance in the same amount of time with same amount of energy dissipated for low frequency $\omega = 0.60\omega_{n_1}$ as with a high frequency $\omega = 1.60\omega_{n_1}$. However, when $a > 0.08$, the system excited with a low frequency $\omega = 0.60\omega_{n_1}$ can travel the fixed distance in less time and with a smaller energy dissipation than the system excited with a frequency $\omega = 1.60\omega_{n_1}$. In other words, when all the other conditions are equal, the excitation with a lower frequency, namely, a longer period, appears to allow the system to take more advantage of the resultant force on the system in the $\mathbf{E}_1$ direction than one with a high excitation frequency.

To illustrate the aforementioned comment about the resultant force in the horizontal direction, we sum the external forces which are composed of friction and damping forces in $\mathbf{E}_1$ direction for the system:

$$\mathbf{F}_{\text{ex}} \cdot \mathbf{E}_1 = \left(\mathbf{F}_{f_1} + \mathbf{F}_{d_1} + \mathbf{F}_{f_2} + \mathbf{F}_{d_2}\right) \cdot \mathbf{E}_1. \tag{17}$$

We next consider the system and subject it to a periodic external force. In the first case, the excitation frequency is sufficiently small that SSL occurs and in the second case the frequency is sufficiently high so that SL occurs. For cases exhibiting SSL and SL, the resultant force $\mathbf{F}_{\text{ex}} \cdot \mathbf{E}_1$ as a function of time are shown in Fig. 10. The sets of results shown in Fig. 10a, b exhibit a similar average speed for the center of mass C. However, the amplitude of force for the SL case in Fig. 10b is almost twice that for the SSL case in Fig. 10a. Since all the parameters except the excitation frequency ω are identical, this effect must be attributed to ω. According to Fig. 10, the period of the resultant force $\mathbf{F}_{\text{ex}} \cdot \mathbf{E}_1$ is half the period of $\ell_0(t)$.

To develop a sense of the role that the period of the resultant external force $\mathbf{F}_{\text{ex}} \cdot \mathbf{E}_1$ in Fig. 10 plays on the motion of the system, we consider a similar scenario of a particle m under the influence of the sawtooth periodic force in the x direction (cf. Fig. 11). The sawtooth profile is an approximation of the profile of $\mathbf{F}_{\text{ex}} \cdot \mathbf{E}_1$ that is visible in Fig. 10b and the particle m can be con-

[1] While the energy e_5 dissipated for $\omega = 0.95\omega_{n_1}$ does decrease after a certain amplitude a is reached, this region in parameter space is not feasible because when the two mass are too close to each other there is a possibility that the normal force on one of them will vanish and that mass would then loose contact with the ground.

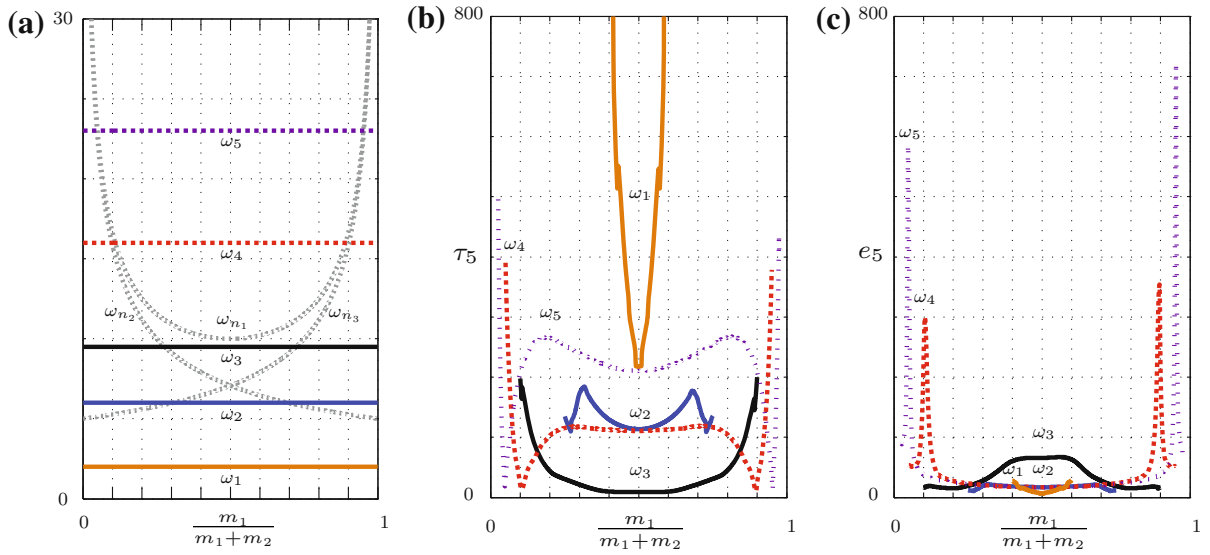

Fig. 12 Numerical results that are used to analyze the energy efficiency of the model in Fig. 4 for different mass distributions $\frac{m_1}{m_1+m_2}$. **a** Natural frequencies $\omega_{n_{1,2,3}}$ as functions of the mass ratio $\frac{m_1}{m_1+m_2}$. **b** Dimensionless time τ_5 to travel a distance of 5 dimensionless units. **c** The corresponding dimensionless energy consumption e_5. The parameters for this model are $k = 50, a = 0.05, \bar{\ell} = 3, d = 0.5, \mu_s = 0.7, \mu_k = 0.5$ and $\omega_1 = 2, \omega_2 = 6, \omega_3 = 9.5, \omega_4 = 16$, and $\omega_5 = 23$, respectively

sidered as the system composed of m_1 and m_2. Based on the above assumption, if the particle of mass m has an initial velocity v_0, then the corresponding average speed $\bar{v}$ in one period of the forcing is

$$\bar{v} = v_0 + \frac{F_{\max} T_f}{6m} = v_0 + \frac{F_{\max}\pi}{3m\omega_f}, \tag{18}$$

where $\omega_f = \frac{2\pi}{T_f}$. Even though the situation in the two-degree-of-freedom model with friction is far more complicated (because the quantities corresponding to F and v_0 are functions of ω_f) we can still use (18) to obtain some qualitative insights. For instance, assuming that $F_{\max}$ and v_0 have the same sign, then Eq. (18) shows that the lower the frequency ω_f, the higher the value we can expect for the average speed $\bar{v}$. This simple model also shows why we should not expect SL to yield faster locomotion than SSL.

5 The effects of mass distribution

The motion of the system is achieved in part by varying the normal forces at the contact points with the ground. These forces are also proportional to the masses m_1 and m_2, respectively. Consequently, it is of interest to examine how the mass distribution $\frac{m_1}{m_2}$ can effect the locomotion of the system. In this section, we examine how the time to travel τ_5 and the energy dissipated e_5 are related to the mass parameter $\frac{m_1}{m_2+m_1}$ for a set of five representative excitation frequencies.

In Fig. 12b, for high frequency $\omega = \omega_5 = 23$, we find three local minima for τ_5 near $\hat{m} = m_1/(m_1 + m_2) = 0.05, 0.95$, and 0.5. When $\hat{m} = 0.05$ or 0.95, then the natural frequency $\omega_{n_1} = \omega$. Like the case shown in Fig. 8, the least time needed to achieve a given distance is near ω_{n_1} and this is produced with maximum energy consumption. We obtain another local minimum in τ_5 when $\hat{m} = 0.5$ (i.e., $m_1 = m_2$) and this is produced with (a local) minimal energy consumption.

The results shown in Fig. 12 provide another way to accelerate our system when changing the excitation frequency is not possible. For $\omega = \omega_4 = 16$, the trend follows what happens with $\omega = \omega_5 = 23$ except the mass ratio where $\omega = \omega_{n_1}$ changes. The third case we consider is $\omega = \omega_3 = 9.5$. Here, as $\omega_3 \approx \omega_{n_1}$ when $m_1 = m_2$, we find that the three valleys reduced to a single wide flat valley. This is a very appealing design region for applications.

If we continue to decrease the excitation frequency to $\omega = \omega_2 = 6$, then the first natural frequency ω_{n_1} can never be reached regardless of the mass distrib-

ution[2]. However, as can be seen from Fig. 12b, we still find three local minima of average velocity at $\hat{m} = 0.27$, 0.73, and 0.5.

As can be seen in Fig. 12a, with the two mass distributions $\hat{m} = 0.27$ and 0.73, the exciting frequencies are quite close to the approximated frequency corresponding to the mode of single mass oscillation $\omega_{n_2} = 5.85$ and $\omega_{n_3} = 5.85$, respectively. For the other minimum at $\hat{m} = 0.5$, the excitation frequency $\omega = \omega_2$ is the closest to ω_{n_1}. Of particular interest to us is that its corresponding energy consumption indicated by Fig. 12c is also a minimum.

The behavior when $\omega = \omega_1 = 2$ follows what occurred with $\omega = \omega_2 = 6$ except that it does not exhibit the two valleys for the travel time τ_5 near the frequency corresponding to a single mass oscillation. By examining numerical simulations for the case $\omega = \omega_1$, we found that SSL was dominant during the entire motion. With one of the masses stuck, we have less energy dissipated. However, the time to reach the fixed distance 5 is longer in general compared to the other cases $\omega_{2,3,4,5,6}$ and is not significantly improved at the minimum $m_1 = m_2$. Finally, when $\omega = \omega_1 = 2$, the system can only be set into motion in a narrow range of mass distributions near $\hat{m} = 0.5$.

6 Conclusions

Based on the numerical simulations and analysis of the simple model, the following conclusions on locomotion can be drawn:

1. SSL typically occurs only for frequencies smaller than $\omega_{n_{1,2,3}}$.
2. SSL is energy efficient, however, it is not always the fastest form of locomotion.
3. During SSL, the time to travel a given distance is not very sensitive to the difference in the coefficients of static and dynamic friction.
4. To achieve the same average velocity of the center of mass, especially when the excitation amplitude a is large, low frequency is better than high frequency in term of energy efficiency.

These observations have potential influence on how friction-controlled robots are operated and designed. The design and operation of these devices include the actuator technology, materials, and geometric dimensions required to achieve the actuation frequency, amplitude, kinetic friction, and mass distribution necessary for energetically efficient locomotion at a prescribed velocity. Such insights have particularly important implications in the design and operation of soft robots. In contrast to their rigid counterparts, soft robots elastically conform to a surface and typically engage in friction-controlled locomotion. Even for designs that cannot be represented by the models examined here, our analysis nonetheless identifies the important factors (e.g., actuation frequency, amplitude) and general advantages of SSL over SL for accomplishing forward motion with minimal frictional energy dissipation.

[2] According to Eq. (11) and Fig. 12a, the minimum ω_{n_1} is 10 with $m_1 = m_2$.

Acknowledgments Support from a Defense Advanced Research Projects (DARPA) 2012 Young Faculty Award to Carmel Majidi is gratefully acknowledged. Xuance Zhou is grateful for the support of a Anselmo Macchi Fellowship for Engineering Graduate Students and a J. K. Zee Fellowship. The authors also take this opportunity to thank an anonymous reviewer for their constructive criticisms.

References

1. Chernous'ko, F.L.: The optimum rectilinear motion of a two-mass system. J. Appl. Math. Mech. **66**(1), 1–7 (2002). doi:10.1016/S0021-8928(02)00002-3
2. Denny, M.: The role of gastropod pedal mucus in locomotion. Nature **285**(1), 160–161 (1980). doi:10.1038/285160a0
3. Donald, B., Levey, C., McGray, C., Rus, D., Sinclair, M.: Power delivery and locomotion of untethered microactuators. J. Microelectromech. Syst. **12**(6), 947–959 (2003). doi:10.1109/JMEMS.2003.821468
4. Driesen, W.: Concept, modeling and experimental characterization of the modulated friction inertial drive (MFID) locomotion principle: Application to mobile microrobots. Ph.D. thesis, École Polytechnique Fédérale de Lausanne (2008). http://infoscience.epfl.ch/record/121454
5. Driesen, W., Rida, A., Breguet, J.M., Clavel, R.: Friction based locomotion module for mobile Mems robots. In: IEEE/RSJ International Conference on Intelligent Robots and Systems, 2007. IROS 2007, pp. 3815–3820 (2007). doi:10.1109/IROS.2007.4399321
6. Edeler, C., Meyer, I., Fatikow, S.: Modeling of stick-slip micro-drives. J. Micro-Nano Mechatron. **6**(3–4), 65–87 (2011). doi:10.1007/s12213-011-0034-9
7. Elder, H.Y.: Peristaltic mechanisms. In: Elder, H.Y., Trueman, E.R. (eds.) Aspects of Animal Movement, vol. 5, pp. 71–92. Society for Experimental Biology, Seminar Series, Cambridge University Press, Cambridge, UK (1985)
8. Frutiger, D., Kratochvil, B., Nelson, B.: MagMites—Microrobots for wireless microhandling in dry and wet

environments. In: 2010 IEEE International Conference on Robotics and Automation (ICRA), pp. 1112–1113 (2010). doi:10.1109/ROBOT.2010.5509678
9. Li, H., Furuta, K., Chernousko, F.: Motion generation of the Capsubot using internal force and static friction. In: 45th IEEE Conference on Decision and Control, pp. 6575–6580 (2006). doi:10.1109/CDC.2006.377472
10. Majidi, C.: Soft robotics: a perspective—current trends and prospects for the future. Soft Robot. **1**(P), 5–11 (2013). doi:10.1089/soro.2013.000
11. McNeil Alexander, R.: Principles of Animal Locomotion. Princeton University Press, Princeton (2003)
12. Murthy, R., Das, A., Popa, D.O.: ARRIpede: a stick-slip micro crawler/conveyor robot constructed via 2.5D MEMS assembly. In: IEEE/RSJ International Conference on Intelligent Robots and Systems, 2008. IROS 2008, pp. 34–40 (2008). doi:10.1109/IROS.2008.4651181
13. Murthy, R., Das, A., Popa, D.O., Stephanou, H.E.: ARRIpede: An assembled die-scale microcrawler. Adv. Robot. **25**(8), 965–990 (2011). doi:10.1163/016918611X568602
14. Nagy, Z., Frutiger, D., Leine, R., Glocker, C., Nelson, B.: Modeling and analysis of wireless resonant magnetic microactuators. In: 2010 IEEE International Conference on Robotics and Automation (ICRA), pp. 1598–1603 (2010). doi:10.1109/ROBOT.2010.5509260
15. Nagy, Z., Leine, R., Frutiger, D., Glocker, C., Nelson, B.: Modeling the motion of microrobots on surfaces using non-smooth multibody dynamics. IEEE Trans. Robot. **28**(5), 1058–1068 (2012). doi:10.1109/TRO.2012.2199010
16. Nakazato, Y., Sonobe, Y., Toyama, S.: Development of an in-pipe micro mobile robot using peristalsis motion. J. Mech. Sci. Technol. **24**(1), 51–54 (2010). doi:10.1007/s12206-009-1174-x
17. Pawashe, C., Floyd, S., Sitti, M.: Modeling and experimental characterization of an untethered magnetic micro-robot. Int. J. Robot. Res. **28**(8), 1077–1094 (2009). doi:10.1177/0278364909341413
18. Seok, S., Onal, C.D., Cho, K.J., Wood, R.J., Rus, D., Kim, S.: Meshworm: A peristaltic soft robot with antagonistic nickel titanium coil actuators. IEEE/ASME Trans. Mechatron. **18**(5), 1485–1497 (2013). doi:10.1109/TMECH.2012.2204070
19. Shepherd, R.F., Ilievski, F., Choi, W., Morin, S.A., Stokes, A.A., Mazzeo, A.D., Chen, X., Wang, M., Whitesides, G.M.: Multigait soft robots. In: Proceedings of the National Academy of Sciences, USA, vol. 108, no. 51, pp. 20400–20403 (2011). doi:10.1073/pnas.1116564108
20. Sitti, M.: Miniature devices: voyage of the microrobots. Nature **458**(7242), 1121–1122 (2008). doi:10.1038/4581121a
21. Suzuki, Y., Li, H., Furuta, K.: Locomotion generation of friction board with an inclined slider. In: 46th IEEE Conference on Decision and Control, 2007, pp. 1937–1943 (2007). doi:10.1109/CDC.2007.4434269
22. Tanaka, Y., Ito, K., Nakagaki, T., Kobayashi, R.: Mechanics of peristaltic locomotion and role of anchoring. J. R. Soc. Interface **9**(67), 222–233 (2012). doi:10.1098/rsif.2011.0339
23. Wood, R.: The first takeoff of a biologically inspired at-scale robotic insect. IEEE Trans. Robot. **24**(2), 341–347 (2008). doi:10.1109/TRO.2008.916997
24. Zimmermann, K., Zeidis, I.: Worm-like locomotion as a problem of nonlinear dynamics. J. Theor. Appl. Mech. **45**(1), 179–187 (2007)